

# Fluidic Stub-Loaded Patch Antenna for Frequency-Tunable Polarization Reconfiguration

ADITYA SINGH<sup>ID</sup> AND CARLOS E. SAAVEDRA<sup>ID</sup>

Department of Electrical and Computer Engineering, Queen's University, Kingston, ON K7L 3N6, Canada

CORRESPONDING AUTHOR: A. SINGH (e-mail: singh.aditya@queensu.ca)

This work was supported in part by the Natural Sciences and Engineering Research Council (NSERC) Strategic Project under Grant STPGP-521223-2018. The work of Aditya Singh was supported by the Ontario Trillium Scholarship Program.

**ABSTRACT** This paper presents a fluidically loaded microstrip patch antenna on a multi-layered substrate with frequency and polarization reconfigurability in the 2400 MHz band. A square patch loaded at all the corners with short circuited  $\lambda_g/4$  long stubs is utilized. An arrangement of fluidic channels fabricated by moulding Polydimethylsiloxane (PDMS) with 3D printed mould is incorporated beneath each stub. By injecting or withdrawing distilled water into the channels, variable loads are realized. It exhibits frequency tunable linearly polarized (LP) mode with symmetric loading or circularly polarized (CP) mode with asymmetric loading. The sense of CP can be switched by swapping the loading configuration along the diagonals of the patch. The equivalent circuit for the antenna is presented. A prototype is fabricated and measured. In LP mode, frequency tuning of 7.85% is achieved. The minimum realized gain is 5.67 dBi with cross-polarization (X-pol) isolation  $\geq 20$  dB. In the CP modes, the overlapping bandwidth for  $|S_{11}| \leq -10$  dB and axial ratio  $\leq 3$  dB (ARBW) is  $\geq 16$  MHz for both LHCP/RHCP modes. Frequency tuning of 141 MHz (5.76%) is measured in the RHCP mode. The minimum realized gain is 4.86 dBi and total efficiency is  $> 60\%$ .

**INDEX TERMS** Patch antenna, circular polarization, dielectric fluid, linear, left-hand circular polarization, right-hand circular polarization, polarization reconfigurable, microfluidics, TM modes, frequency tunable, distilled water.

## I. INTRODUCTION

FLUIDIC antennas have received considerable attention among researchers due to their reconfigurability potential and advancements in microfluidic fabrication technology [1], [2]. They either utilize conductive fluids such as liquid-metal [3] or dielectric fluids. Recently, liquid dielectric-based antennas have become popular since they offer advantages such as low cost, easy reconfigurability, biocompatibility, and conformability [4]. Numerous works have reported antennas that utilize dielectric fluids as the main radiator such as fluidic monopoles [5], [6], [7], dielectric resonator antennas (DRAs) [8], [9], [10], fluidic spiral [11] and helical antennas [12], microstrip dielectric patches [13], [14], [15], among others [16], [17]. Alternatively, dielectric fluids inside microfluidic channels have been shown to alter the characteristics of planar antennas including their operating frequency [18], [19], [20], radiated pattern [21], [22], or polarization [23], [24].

Fluidics has also been applied to design polarization reconfigurable antennas. In [11], distilled water is used to replace the metallic arms in a archimedian spiral using two glass arms. These arms are flared out in an inverse fashion to redirect the currents in opposite directions by filling either arm to produce either left-hand circularly polarized (LHCP) or right-hand circularly polarized (RHCP) radiations. A large ground plane with a wideband parallel stripline feed is utilized to achieve static axial ratio bandwidth (ARBW) of 40%. Authors in [12] proposed a polarization reconfigurable helical antenna with water replacing the metallic arms. Two water helices with counter rotational directions are placed nearly overlapping each other. When water is contained in the one helix, RHCP radiation is obtained while LHCP radiation is achieved when water is filled in the second helix instead. It exhibits an ARBW of 50.3%. However, [11] and [12] cannot obtain linear polarization (LP). Furthermore, [23] presents an antenna loaded with a variable height water

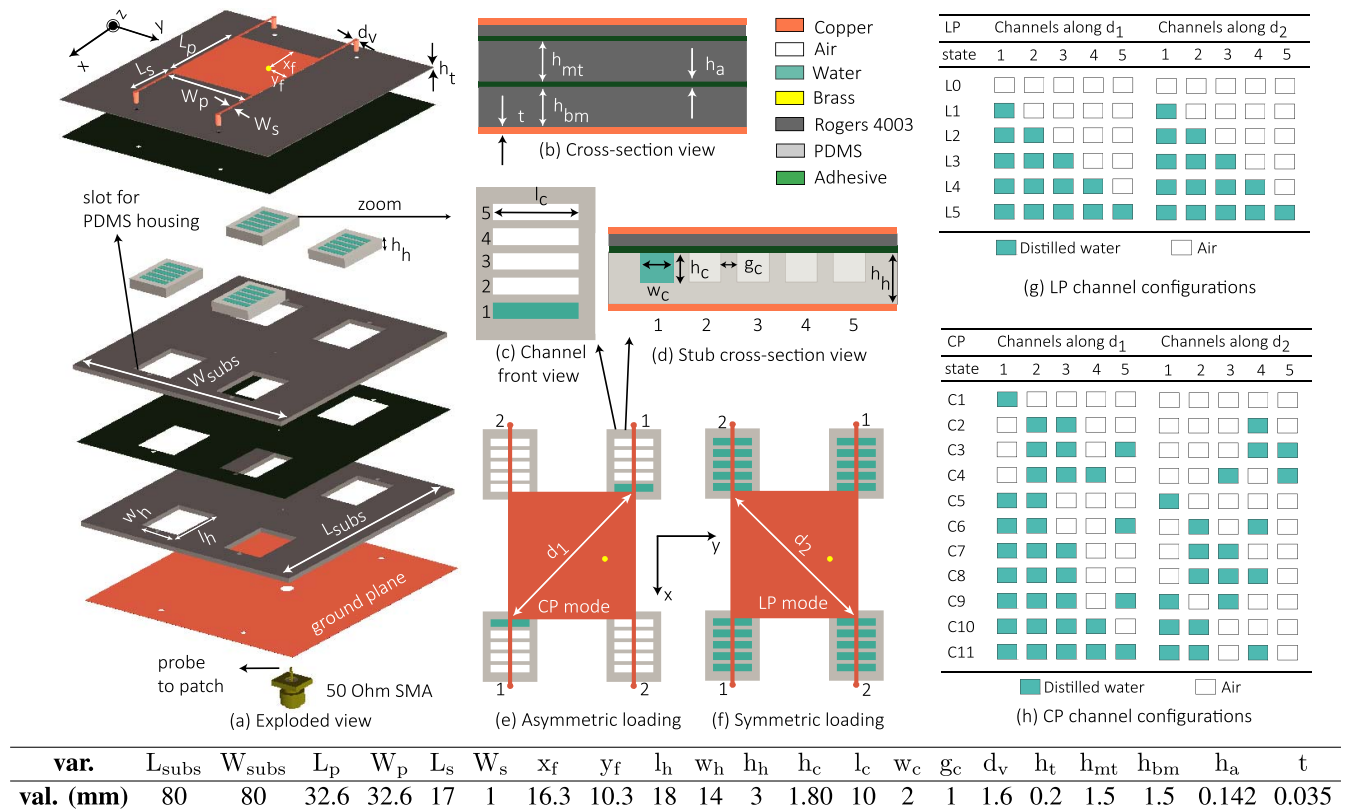


**FIGURE 1.** Antenna structure and design: (a) Exploded view of the multi-layered patch antenna, (b) Cross-section view showing various layers, (c) Front view of the PDMS housing with fluidic channels, (d) Cross-section of Fluidic load, (e) Antenna loading in RHCP state C1, (f) Antenna loading in LP state L5, (g) Channel configuration in LP states, (h) Channel configuration in CP states.

column using tubes directly on the corners of a microstrip patch to obtain frequency-tunable polarization reconfiguration. Injecting water into the tubes loads the patch antenna and shifts the resonant frequencies of the patch's degenerate modes. Equal fluid level on all four tubes results in LP with 4.6% measured tuning range. Unequal fluid levels give LH/RH CP to yield an ARBW of 0.39% and measured tuning range of 3.6% in the CP mode. In [9], a probe-fed water DRA uses an acrylic holder divided into 4 sections and any two are injected with water. When the water is filled symmetrically around the probe, LP is obtained. Alternatively, CP is obtained with asymmetric filling around the probe exciting two dielectric resonator antenna (DRA) modes in phase quadrature. The antenna exhibits ARBW of 22% with profile being  $> \lambda_0/4$ .

This paper presents a probe-fed microstrip patch antenna with frequency-tunable polarization reconfigurability. The antenna is designed on a multi-layered substrate and employs fluids to load a square patch antenna using short circuited quarter-wave long stubs. These stubs use a modified substrate that incorporates five fluidic channels. The channels are identical and equally spaced and filled with fluid (distilled water) in a digital manner (filled or vacant) to alter the electrical length of the stubs. The antenna works in three modes with frequency tuning – LP mode with symmetric loading

along both the diagonals of the square patch or CP mode (LHCP/RHCP) with asymmetric loading along the diagonals of the patch. The sense of CP can be switched by swapping the channel filling configurations along the diagonals. The channel dimensions are tuned such that near-continuous tuning range is achieved in all three modes. We first describe the design, working principle, and operating modes of the antenna followed by deriving an electrical circuit equivalent for the proposed tuned antenna. Subsequently, the experimental validation of the concept with a fabricated prototype is presented.

## II. DESIGN PRINCIPLE

### A. ANTENNA STRUCTURE AND RECONFIGURABILITY

The exploded view of the reconfigurable antenna is shown in Fig. 1 (a). A square microstrip patch antenna is employed as the reference for the reconfigurable design. A multilayered substrate is employed using Rogers 4003 ( $\epsilon_r = 3.55$  and  $\tan \delta = 0.0027$ ) namely the top, middle and bottom substrate layers joined together as shown in Fig. 1 (b). The thickness of the top layer is 0.2 mm while other layers are 1.5 mm thick. The antenna structure is printed on the top layer while the ground plane is printed on the bottom layer. Probe feeding is used to connect a 50  $\Omega$  SMA connector to the patch.

To add reconfigurability all the corners of the patch are attached to quarter-wave long stubs printed on the top layer. The stubs are short circuited to the ground plane using metallic vias. The multilayered substrate beneath each stub is modified by cutting out a rectangular slot ( $l_h \times w_h$ ) in the middle and bottom substrates to incorporate fluidic channels while the top substrate remains intact. Five identical and equally spaced fluidic channels created in Polydimethylsiloxane (PDMS) housings are incorporated as shown in Fig. 1 (c). This provides the ability to apply individual loadings along each diagonal of the patch by injecting or withdrawing the fluid from the channels. The fluid used is distilled water ( $\epsilon_r = 78.7$  and  $\tan \delta = 0.13$  at  $20^\circ\text{C}$  at 2400 MHz) [25].

A square patch antenna supports two degenerate lowest order modes namely  $\text{TM}_{10}^z$  and  $\text{TM}_{01}^z$ , where, the subscripts define the number of half cycles in the field distribution along the  $x$  and  $y$  direction using the coordinate system defined in Fig. 1 (a). The antenna is linearly polarized with one mode dominating along one principal plane and vice-versa. Furthermore, loading the patch modes with variable reactive loads shifts the resonance frequency of the modes. For example, loading the patch along diagonal  $d_1$  shifts the frequency of  $\text{TM}_{10}^z$  while loading along  $d_2$  affects  $\text{TM}_{01}^z$ . Therefore, loading the patch equally along both the diagonals affects both the modes equally and hence LP is preserved. However, asymmetric loading along the diagonals results in splitting of the degenerate modes and CP radiation can be achieved between the resonant frequencies of the modes [26].

### B. FLUIDICALLY LOADED STUB

The reactive loading is realized by using the short circuited stubs. The stubs are designed to be  $\lambda_g/4$  long at 2790 MHz, where  $\lambda_g$  is the guided wavelength in the microstrip environment [27]. Hence, at resonance, it looks like an open circuit while below resonance it is inductive and above it is capacitive. The electrical length of the stub is modified by injecting the fluid in the channels. Since, distilled water has much larger relative permittivity ( $\sim 80$ ) than PDMS ( $\sim 2.1$ ) or air ( $\sim 1$ ), the resonant frequency shifts downward and the stub appears electrically longer. Notably, distilled water provides high contrast in the dielectric constant value, hence the effective dielectric constant of the modified substrate can be increased with smaller volume of fluid. Thus, the fluid volume is easier to handle. Furthermore, since water is chemically inert to most of the materials it is a safer choice compared to other organic fluids such as acetone, ethyl alcohol and ethyl acetate. Moreover, due to the short circuit at the via end, the  $\mathbf{E}$ -field is minimum near the via end while it is maximum at the open end (attached to the patch). The fluidic channels created in the PDMS housings are evenly distributed from the open end to the via end. The position of the fluidic channel must be closest to the copper traces as it has most profound effect on local  $\mathbf{E}$ -field in this case, thus the top layer is kept very thin. Also, the width ( $w_c$ ) and the depth ( $h_c$ ) of the channel are critical in

obtaining a desired frequency shift since it determines how much volume is replaced by the fluid between the signal and the ground plane. Larger water volume results in a higher effective permittivity and shifts the resonance downwards. The channel beneath the open end has strongest effect due to presence of stub's  $\mathbf{E}$ -field maxima, inducing largest shift. The gap ( $g_c$ ) between the channels controls the position and the number of channels that can be added below the stub. As  $g_c$  is reduced, the channels are tightly placed near the open end, inducing larger frequency shift and further providing space for more channels. This can provide higher tuning range, however, for robustness and ease of fabrication,  $g_c$  is optimized at 1 mm.

### C. LINEARLY AND CIRCULARLY POLARIZED MODES

In the LP mode, the operational frequency of the antenna can be tuned by varying the loading symmetrically on the patch antenna. When the stubs on the patch are not present the resonance occurs at 2418 MHz. After introduction of the stub with all channels vacant (air filled), the resonance frequency shifts to a higher frequency. An upward shift in the resonance to 2546 MHz is observed since the stub looks like an inductive load in the vicinity of patch resonance. As the channels are filled from channel 1 to 5, the operation frequency shifts downwards due to loading effect.

In the CP mode, the antenna is loaded asymmetrically along the two diagonals. Thus, the shift in resonance frequency of the  $\text{TM}_{10}^z$  and  $\text{TM}_{01}^z$  are unequal. If the resonance frequencies of the modified  $\text{TM}_{10}^z$  and  $\text{TM}_{01}^z$  modes are  $f'_{10}$  and  $f'_{01}$ , the center frequency for CP operation is between the two frequencies [28]. From now onwards, the modified  $\text{TM}_{10}^z$  and  $\text{TM}_{01}^z$  modes would be called as orthogonal modes mode 1 and mode 2 with frequencies  $f_1$  and  $f_2$ . The dimensions of the fluidic channel are tuned such that the induced frequency shift between mode 1 and mode 2 is large enough to resolve the modes when one only channel is filled (see Fig. 1 (e)) but small enough to maintain continuous tuning in LP and CP modes. Depending on the various channel filling options, the LP mode configurations are given in Fig. 1 (g) while the set of best axial ratio (AR) performing channel filling configurations are shown in Fig. 1 (h) for the RHCP mode. The sense of CP radiation is dependent upon the loading condition. For example stronger loading along  $d_1$  results in RHCP radiation in the far field while equal and opposite loading produces LHCP radiation. Since, both RHCP/LHCP modes require fluidic loadings which are mirror image of each other only RHCP results will be discussed in detail while LHCP discussion will be limited. A detailed discussion of the CP mode performance is provided in Section IV.

### III. EQUIVALENT CIRCUIT ANALYSIS

The behavior of the antenna under various loading conditions can be modelled using a lumped equivalent circuit (LEM) of the antenna and transmission line model (TLM) for the fluidically loaded stub as shown in Fig. 2 (a) and (b). The parallel RLC circuit model for the first order degenerate modes is

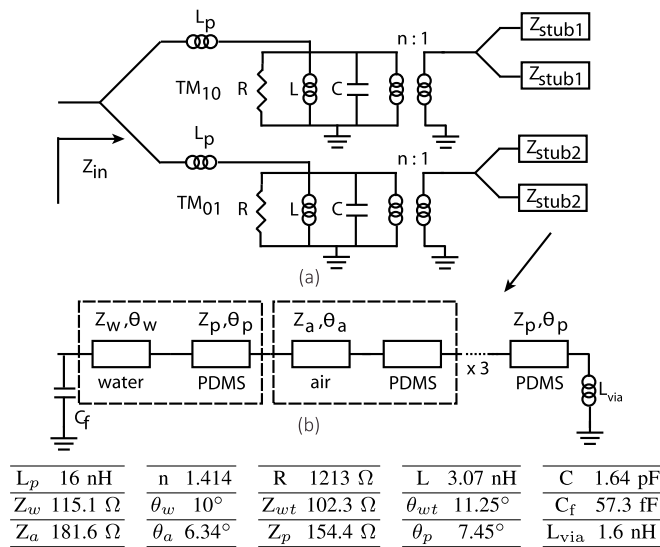
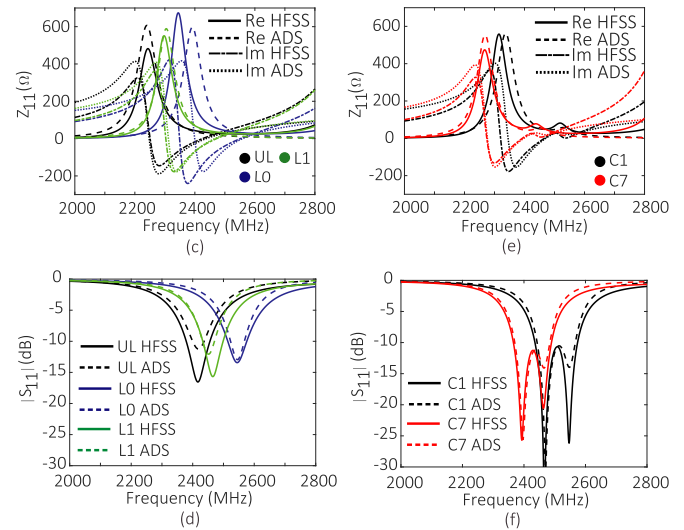


**FIGURE 2.** Results for equivalent electrical circuit analysis: (a) First order antenna equivalent circuit with degenerate modes in parallel loaded with stub's TL model, (b) Fluidically loaded stub modelled as multi-section TL. Full-wave simulations and equivalent circuit simulations for the antenna in unloaded (UL) antenna and LP states (L0 and L1) shown in (c)  $Z_{11}$  response and (d)  $|S_{11}|$  response. Full-wave simulations and equivalent circuit simulations for the antenna in two RHCP states (C1 and C7) shown in (e)  $Z_{11}$  response and (f)  $|S_{11}|$  response.

extracted using the unloaded antenna. The inductance  $L_p$  represents the probe inductance and the higher order modes. The shorting via is modelled as an inductor [29] where equivalent inductance is given as  $L_{via} = 5.08 \log_{10}(\frac{4h}{d} - 1)$ . The stub is modelled as a multi-section transmission line that uses a multi-layered substrate. The equivalent dielectric permittivity of the multilayered substrate is modelled using the formulas given in [30]. As a result, the fluidic stub impedance ( $Z_{stub}$ ) is modelled as a combination of water, air, and PDMS loaded lines as shown in Fig. 2 (b). The characteristic impedance and the electrical length ( $Z_{w,a,p}$  and  $\theta_{w,a,p}$ ) of each section is calculated using the effective permittivity calculated using [30]. Thus, depending upon the design parameters of the fluidic channels namely  $h_c$ ,  $w_c$ , and  $g_c$ , the characteristic impedance and electrical length  $Z_{w,a,p}$  and  $\theta_{w,a,p}$  of the loaded line section can be tuned. The transition between the patch and the stub is modelled using the transformer with turn ratio  $n:1$ . Since, the first channel lies beneath the patch corner an additional capacitance  $C_f$  is added. The model parameters such as  $n$ ,  $Z_w$ ,  $\theta_w$  and  $C_f$  are tuned to fit the  $S_{11}$  and  $Z_{11}$  curves for the water unloaded antenna (L0 state) and loaded antenna in the C1 state. The final tuned parameters are shown in the Fig. 2 where  $Z_{wt}$ ,  $\theta_{wt}$  show tuned values and each electrical length  $\theta$  defined at 2400 MHz for 2 mm wide channel. The stub impedance  $Z_{stub1}$  and  $Z_{stub2}$  are the same and hence produce equal shifts in resonance in the LP mode. The  $Z_{11}$  and  $|S_{11}|$  curves for various conditions is shown in Fig. 2 (c) and (d). In general, there is a good agreement between the modelled and full-wave trends, hence, the model can be used as a starting point for design parameters of the channels.

When the loads  $Z_{stub1}$  and  $Z_{stub2}$  are distinct, the modes are separated due to different resonant frequencies. The



comparison between the modelled and full-wave results for RHCP states C1 and C7 are shown in Fig. 2 (e) and (f). It is seen that the  $|S_{11}|$  and  $Z_{11}$  responses correlate well. The slight differences may be caused due to some higher order electromagnetic (EM) effects. Only selected states are shown for brevity, in general similar trend is observed for other states in LP and RHCP/LHCP modes.

## IV. EXPERIMENTAL RESULTS

### A. ANTENNA PROTOTYPE FABRICATION

The prototype antenna is fabricated using one thin and two thick pieces of Rogers 4003 substrate. In the top layer, the antenna structure is patterned on copper cladding of the 0.2 mm substrate using a LPKF ProtoMat E44 circuit plotter. The cladding on the other side is removed. The middle layer is a 1.5 mm thick substrate with the claddings peeled off on both the sides. Finally, for the bottom substrate, the top cladding is removed while the bottom cladding serves as the ground plane. Further, to position the PDMS housing with fluidic channels, rectangular slots are cut in the bottom and middle layers. All layers are joined together using ARseal 90880 polypropylene double-sided adhesive tape with excess tape removed around the slots. A 50  $\Omega$  SMA connector is used to feed the patch using probe feed as shown in Fig. 3 (a) and (b). The fluidic channels in PDMS are created using a silicone elastomer kit and two holes with a diameter of 0.5 mm are created in each channel to allow for fluid inlet/outlet. Fluid is injected and withdrawn using syringes and copper tape is often removed and applied again after each tested CP/LP state. This is done for quick prototyping and proof of concept. Ideally, another thin substrate with holes drilled along the channel ports can be used to realize the ground plane as shown in Fig. 3 (c).

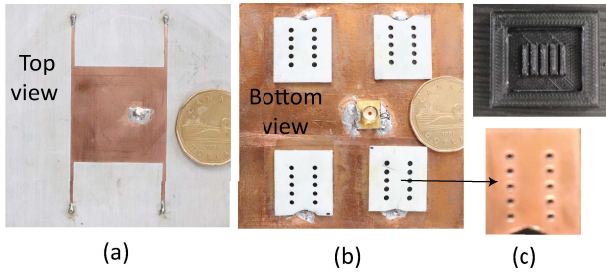


**FIGURE 3.** Picture of fabricated antenna (a) Top view, (b) Bottom view (c) 3D printed mould and cover back view.

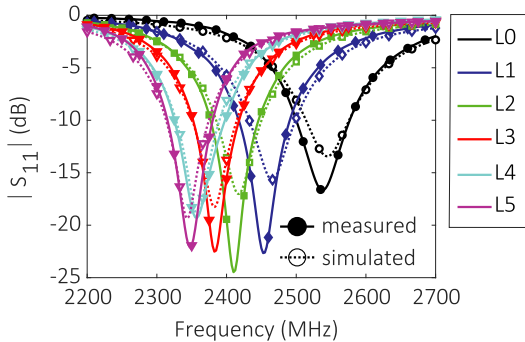


**FIGURE 4.** Simulated and measured  $|S_{11}|$  responses in various LP states.

### B. S PARAMETER RESPONSE

The measured and simulated  $S_{11}$  responses for the antenna in the LP mode are shown in Fig. 4. When channel 1 is filled with fluid along both the diagonals it causes the largest shift in the simulated response equal to 80 MHz. Simulations show that consecutively injecting the fluid to channels 2, 3, 4, and 5 leads to states L2, L3, L4, and L5 with frequency shifts of 49 MHz, 35 MHz, 25 MHz, and 14 MHz respectively. As more channels are filled from the open end of the stub towards the shorted end, the amount of frequency shift is reduced. This is because, the frequency shift depends on the reactive impedance change of the stub which in turn depends on the E-field distribution on the stub. Fluid-loading locally disturbs the existing E-field on the stub making the fluid loading effect position dependent. The channel below the open end has the greatest impact while the one near the shorted end has the least impact. This phenomenon is important in tuning the CP modes to achieve the target AR in the desired frequency band.

The  $S_{11}$  responses for the antenna in the CP modes are shown in Fig. 5. The responses for different states are split up and shown in different subfigures for better clarity. The first step to change the antenna polarization from LP to CP is to change the fluid loading from symmetric to asymmetric. In the RHCP state C1 as shown in Fig. 5 (a), channel 1 along  $d_1$  is filled while all the channels along  $d_2$  are vacant as seen in Fig. 1 (e). As a result, the mode 1 shifts downward while the mode 2 remains intact. The minimum AR is obtained near arithmetic mean of the two resonant frequencies. For example in state C1,  $f_1 = 2470$  MHz and  $f_2 = 2550$  MHz,

then  $f_0 = 2510$  MHz where the AR is minimum. The separation between the two frequencies cannot be too large as the  $S_{11} \leq -10$  dB is not met due to limited bandwidth (high  $Q_0$ ) offered by reference patch antenna [31]. Based on the antenna's unloaded quality factor ( $Q_0$ ), the separation between the two frequencies can be chosen [26]. A higher  $Q_0$  requires that the two frequencies remain closer and hence the loading needs to be reduced. The unloaded  $Q_0$  for our design is  $\sim 25$  and thus it is required to have two frequencies between 50 MHz to 100 MHz apart for a good CP performance. To tune the CP mode response to lower frequency, either both the modes can be tuned downwards or the separation between them can be reduced. In state C2,  $f_1 = 2476$  MHz and  $f_2 = 2525$  MHz, then  $f_0 = 2500.5$  MHz. This is done by using the configuration for state C2. Similarly, to bring down the CP mode frequency, the loading along  $d_1$  and  $d_2$  are increased while keeping the separation between  $f_1$  and  $f_2$  around 40–80 MHz by injecting fluid into different fluidic channels. For all the selected CP states, the loading configurations are shown in Fig. 1 (h).

Furthermore, the electric field distribution on the patch antenna and the stubs at 2514 MHz for the RHCP state C1 is shown in the Fig. 6. With the advancement of excitation phase, the effective magnetic current circulates along the periphery of the patch. For example, at  $\omega t = 0^\circ$ , the E-field cancels along the x-direction while it results in an effective magnetic current along y-direction. When  $\omega t = 90^\circ$ , the effective magnetic current results along the x-direction. A similar observation can be made when  $\omega t$  is  $180^\circ$  and  $270^\circ$ . Thus, this results in currents that are in phase quadrature and have nearly equal magnitudes, resulting in CP radiation.

### C. FAR FIELD RESPONSE

The far field response is measured inside an anechoic chamber at Queen's University. The peak realized measured gain for states L0, L2, and, L4 is 6.0, 5.67, and 5.96 dBi respectively. The total efficiency measurement was carried out using improved Wheeler's cap method in [32]. The measured total efficiency in LP mode is  $-2.11$  to  $-0.84$  dB (61.5% - 82.4%). The measured tuning range (TR) is 7.85% as shown in Fig. 7 (a). The normalized radiation patterns are plotted in Fig. 8 (a) for three states namely L0, L2, and L4 in the xz and yz planes. The simulated and measured radiation pattern show good agreement and the minimum measured cross-polar (X-pol) isolation is around 20 dB in the broadside direction.

In the CP mode, the far field measurements are done by measuring both the amplitude and phase response using a vector network analyzer and a LP horn antenna as the transmitter. The magnitude and phase of the received signal is recorded by rotating the LP horn from vertical to horizontal polarization. The calculations for the RHCP, LHCP received power, AR, gain calculations are done using the method given in [33]. The simulated and measured tunable AR performance is shown in Fig. 5 (e) and (f) respectively for the

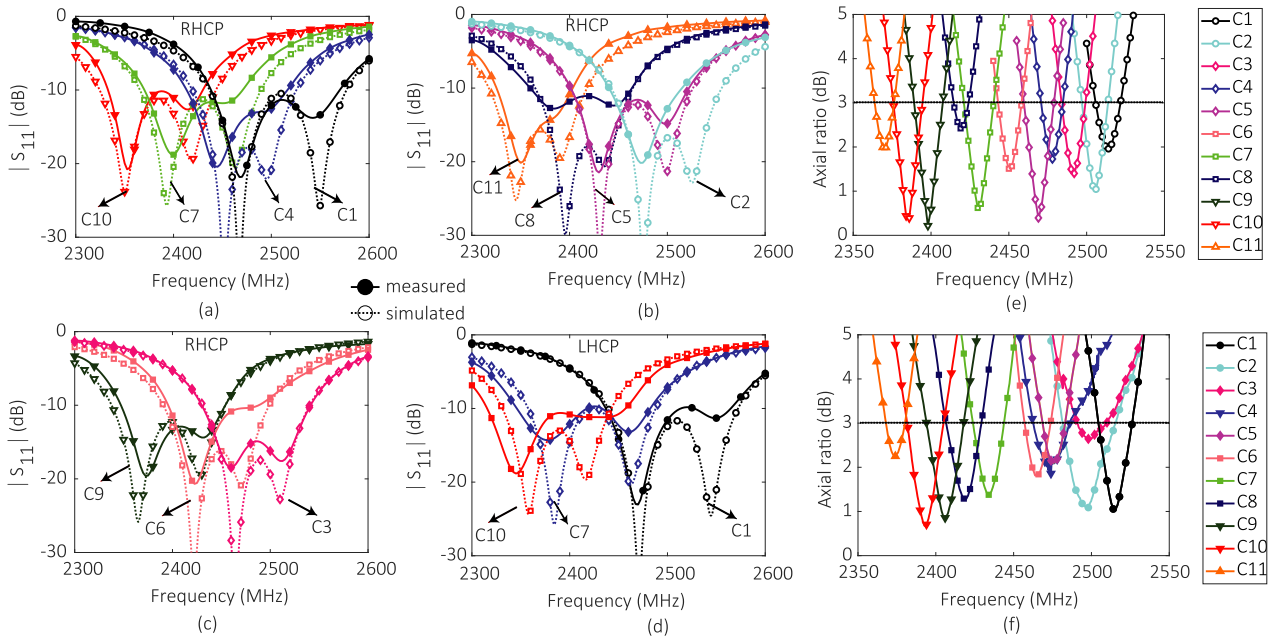


**FIGURE 5.** Measured  $|S_{11}|$  (a to d) and axial ratio (e, f) responses for the proposed antenna in various CP states. (a) RHCP states C1, C4, C7, and C10, (b) RHCP states C2, C5, C8, and C11, (c) RHCP states C3, C6, and C9, (d) LHCP states C1, C7, and C10, (e) Simulated AR RHCP, (f) Measured AR RHCP.

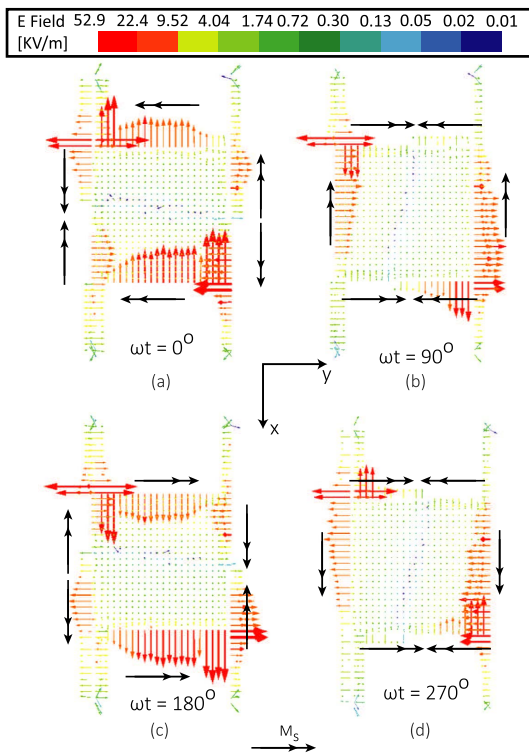


**FIGURE 6.** Electric field distribution on the patch and stubs in the RHCP state C1 for various input phases ( $\omega t$ ) at 2514 MHz.  $M_s$  is magnetic current source. (a)  $\omega t = 0^\circ$ , (b)  $\omega t = 90^\circ$ , (c)  $\omega t = 180^\circ$ , (d)  $\omega t = 270^\circ$ .

RHCP mode. Frequency tuning of 141 MHz (5.76%) is measured. The measured average ARBW for RHCP/LHCP states is 20.1 and 20.7 MHz respectively. Finally, the measured total efficiency in RHCP mode is  $-2.18$  to  $-1.34$  dB (60.5% – 73.4%) as shown in Fig. 7 (b). Notably, the efficiency of the

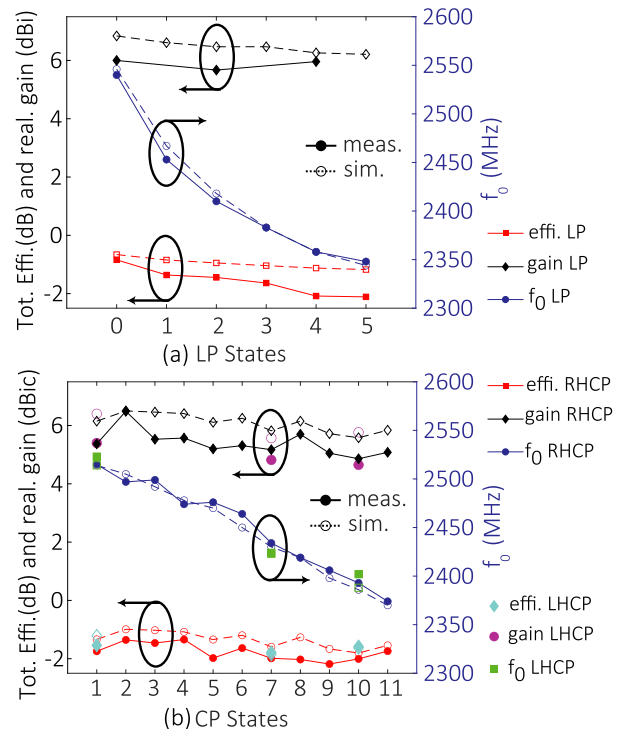


**FIGURE 7.** Antenna performance showing total efficiency, realized gain and center frequency  $f_0$  in various states. (a) LP mode, (b) CP mode.

antenna drops slightly if channel 1 along either or both the diagonals is injected with water since it is located directly beneath the radiating patch.

The radiation pattern is measured at selected states which span the whole tuning range namely C1, C7, and C10. The

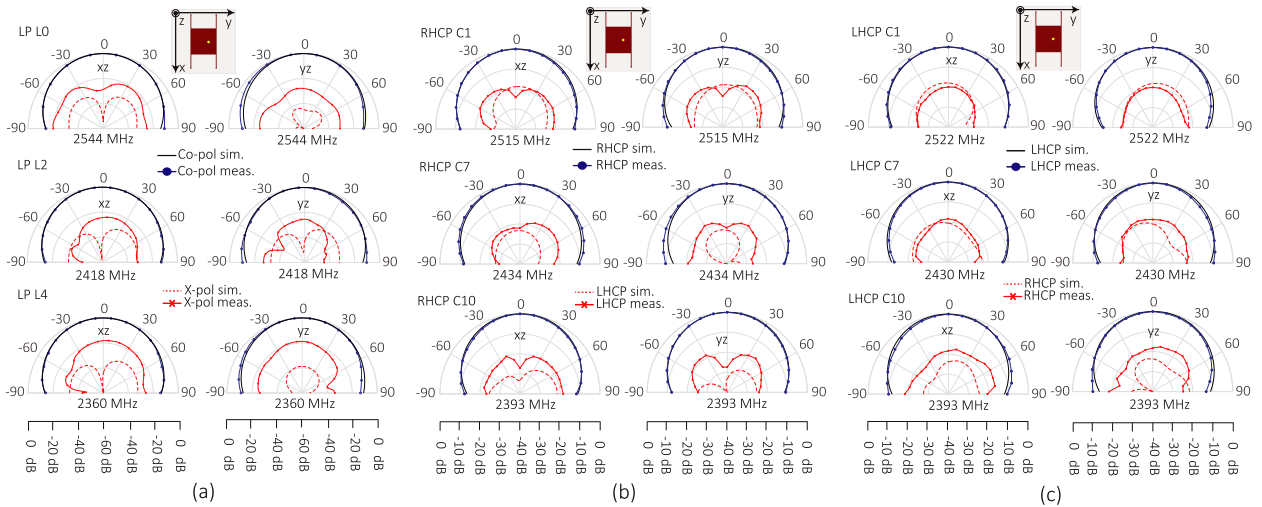


**FIGURE 8.** Normalized measured radiation pattern for the proposed reconfigurable antenna. (a) LP states (L0, L2, L4), (b) RHCP states (C1, C7, C10), (c) LHCP states (C1, C7, C10). Left and right columns in each subfigure show patterns in xz and yz planes respectively.

**TABLE 1.** Comparison with other liquid-based polarization reconfigurable antennas.

Ref.	Ant. Type	$f_0$ (MHz)	Profile ( $\lambda_0$ )	size. ( $\lambda_0^2$ )	ARSBW (%)	CP Gain (dBi)	LP Gain (dBi)	CP (%)	Effi. (%)	LP (%)	Effi. (%)	CP TR (%)	LP TR (%)	Polarization recon.
[9]	water DRA	2620	>0.32	1.71	22.1	$\leq 4.2$	$\leq 3.8$	58 - 73	58 - 72	NT	NT	NT	NT	LP/RHCP/LHCP
[11]	water spiral	1500	0.124	2.25	40	6.3 - 8.6	-	NA	-	-	-	NT	-	RHCP/LHCP
[15]	water patch	1960	>0.3	0.72	8.0	$\leq 3.05$	-	$\leq 48$	-	-	-	NT	NT	LHCP only
[23] <sup>a</sup>	microstrip patch	950	0.042	0.18	0.39	$\sim 6$	$\sim 6$	>75	>75	3.60	4.6	NT	NT	LP/RHCP/LHCP
[24] <sup>a</sup>	microstrip slot	2450	0.090	0.96	3.18	1.04-5.86	$\leq 4.25$	NA - 41	NA	NT	NT	NT	NT	LP*/RHCP/LHCP
This	microstrip patch	2440	0.028	0.42	0.82	4.86 - 6.49	5.67 - 6.0	60.5 - 73.4 <sup>b</sup>	61.5 - 82.4 <sup>b</sup>	5.76	7.85	5.76	7.85	LP/RHCP/LHCP

NA = not available, NT = not tunable,  $f_0$  = center frequency, <sup>a</sup>only limited data available, \*Low overlap between LP and CP, <sup>b</sup>includes mismatch loss

normalized radiation pattern for the CP states is shown in Fig. 8 (b) for RHCP and Fig. 8 (c) for the LHCP mode showing reasonable agreement with simulations. The peak realized measured gain are 5.37, 5.17, and 4.86 dBic for states C1, C7, and C10 in the RHCP mode and 5.41, 4.82, 4.65 dBic for states C1, C7, and C10 in the LHCP mode. Overall, good performance is validated in the LP/CP modes and the summary of performance is provided in Fig. 7 (a) and (b).

A comparison with other liquid-based antennas is provided in Table 1. The proposed antenna shows improved performance compared to liquid-based antennas with same reconfiguration capability with a low profile. The other antennas show higher CP bandwidth but with reduced gain [9], significantly larger antenna volume or reduced reconfigurability [11], [15], [24]. The measured tuning range (TR) in CP and LP modes is 5.76% and 7.85% respectively. Since, the achievable BW for reference patch is restricting, the fluid channel parameters such as the size and depth were set to reduce the amount of loading on the patch in order to obtain continuous CP tuning and obtain a decent TR. The TR can be increased by improving the static ARBW of the reference patch antenna by using engineered ground plane [31] and/or introducing an larger air layer in place of middle substrate [34]. Once wider BW is achieved, the loading on the patch can be increased by using more stubs/fluid, thus, increasing the continuous TR. Finally, the idea of using a variable reactive loading can be extended in the future to

other planar antenna types with higher bandwidth such as monopoles [35].

## V. CONCLUSION

A fluidically reconfigurable microstrip patch antenna with frequency and polarization tuning has been proposed and validated. The antenna works in two frequency-tunable modes – linearly polarized mode and reconfigurable circularly polarized mode with LHCP/RHCP. The antenna reconfigures by employing fluidic stub loading along the diagonals of the patch using five fluidic channels fabricated with PDMS. The channels are filled in digital manner (either filled or vacant). Furthermore, all the states in the CP mode utilize a fluidic loading scheme where the two stubs along a given diagonal are identical. Thus, if automated setup is utilized then the fluid inlets and outlets along one diagonal could be combined to be driven by fluidic micropump and a 1 to 10 demux fluidic switch. Finally, all the measured results from the fabricated prototype show a reasonable match with simulated results. The deviation from simulated result may be caused due to difference in material properties, fabrication tolerances, and incomplete channel filling inside the fluidic channels which may improve with hermetic sealings and micropumps.

## REFERENCES

- [1] Y. Temiz, R. D. Lovchik, G. V. Kaigala, and E. Delamarche, "Lab-on-a-chip devices: How to close and plug the lab?" *Microelectron. Eng.*, vol. 132, pp. 156–175, Jan. 2015.

- [2] K. N. Paracha, A. D. Butt, A. S. Alghamdi, S. A. Babale, and P. J. Soh, "Liquid metal antennas: Materials, fabrication and applications," *Sensors*, vol. 20, no. 1, p. 177, 2020.
- [3] K. Khoshmanesh *et al.*, "Liquid metal enabled microfluidics," *Lab Chip*, vol. 17, no. 6, pp. 974–993, 2017.
- [4] E. Motovilova and S. Y. Huang, "A review on reconfigurable liquid dielectric antennas," *Materials*, vol. 13, no. 8, p. 1863, 2020.
- [5] C. Borda-Fortuny, L. Cai, K. F. Tong, and K. Wong, "Low-cost 3D-printed coupling-fed frequency agile fluidic monopole antenna system," *IEEE Access*, vol. 7, pp. 95058–95064, 2019.
- [6] M. Wang and Q.-X. Chu, "High-efficiency and wideband coaxial dual-tube hybrid monopole water antenna," *IEEE Antennas Wireless Propag. Lett.*, vol. 17, no. 5, pp. 799–802, May 2018.
- [7] C. Hua, Z. Shen, and J. Lu, "High-efficiency sea-water monopole antenna for maritime wireless communications," *IEEE Trans. Antennas Propag.*, vol. 62, no. 12, pp. 5968–5973, Dec. 2014.
- [8] J. Ren *et al.*, "Radiation pattern and polarization reconfigurable antenna using dielectric liquid," *IEEE Trans. Antennas Propag.*, vol. 68, no. 12, pp. 8174–8179, Dec. 2020.
- [9] M. Wang and Q.-X. Chu, "A wideband polarization-reconfigurable water dielectric resonator antenna," *IEEE Antennas Wireless Propag. Lett.*, vol. 18, no. 2, pp. 402–406, Feb. 2019.
- [10] M. Zou, Z. Shen, and J. Pan, "Frequency-reconfigurable water antenna of circular polarization," *Appl. Phys. Lett.*, vol. 108, no. 1, 2016, Art. no. 014102.
- [11] Z. Hu, S. Wang, Z. Shen, and W. Wu, "Broadband polarization-reconfigurable water spiral antenna of low profile," *IEEE Antennas Wireless Propag. Lett.*, vol. 16, pp. 1377–1380, Dec. 2017, doi: [10.1109/LAWP.2016.2636923](https://doi.org/10.1109/LAWP.2016.2636923).
- [12] Z. Ren, S.-S. Qi, Z. Hu, Z. Shen, and W. Wu, "Wideband water helical antenna of circular polarization," *IEEE Trans. Antennas Propag.*, vol. 67, no. 11, pp. 6770–6777, Nov. 2019.
- [13] M. M. Abdelbary, H. A. Malhat, and S. H. Zainud-Deen, "Circularly polarized reconfigurable water based microstrip antenna," in *Proc. 36th Nat. Radio Sci. Conf. (NRSC)*, 2019, pp. 44–51.
- [14] Y. Li and K. Luk, "A water dense dielectric patch antenna," *IEEE Access*, vol. 3, pp. 274–280, 2015.
- [15] J. Sun and K.-M. Luk, "A circularly polarized water patch antenna," *IEEE Antennas Wireless Propag. Lett.*, vol. 19, no. 6, pp. 926–929, Jun. 2020.
- [16] N. Brennan, G. H. Huff, B. Rupp, M. A. Bevan, S. A. Long, and W. M. Dorsey, "A fluidic-enabled polarization reconfigurable antenna on a hexagonal substrate tile," in *Proc. IEEE Antennas Propag. Soc. Int. Symp. (APSURSI)*, 2013, pp. 1642–1643.
- [17] S. Wang, Z. Hu, W. Wu, and Z. Shen, "A low-profile frequency and polarization reconfigurable circularly polarized water antenna for satellite navigation," in *Proc. IEEE Int. Symp. Antennas Propagat. (APSURSI)*, 2016, pp. 1507–1508.
- [18] A. Singh, I. Goode, and C. E. Saavedra, "A multistate frequency reconfigurable monopole antenna using fluidic channels," *IEEE Antennas Wireless Propag. Lett.*, vol. 18, no. 5, pp. 856–860, May 2019.
- [19] A. Singh and C. E. Saavedra, "A frequency-reconfigurable water-loaded planar monopole antenna," in *Proc. 18th Int. Symp. Antenna Technol. Appl. Electromagn. (ANTEM)*, 2018, pp. 1–4.
- [20] A. Singh and C. Saavedra, "Fluidically reconfigurable MIMO antenna with pattern diversity for sub-6-GHz 5G relay node applications," *Can. J. Electr. Comput. Eng.*, vol. 43, no. 2, pp. 92–99, 2020.
- [21] I. Goode and C. Saavedra, "A four element phased patch antenna array using fluidic phase shifter," in *Proc. URSI Gen. Assembly Sci. Symp.*, Montréal, QC, Canada, 2017, pp. 1–2.
- [22] J.-J. Liang, G.-L. Huang, K.-W. Qian, S.-L. Zhang, and T. Yuan, "An azimuth-pattern reconfigurable antenna based on water grating reflector," *IEEE Access*, vol. 6, pp. 34804–34811, 2018.
- [23] Y. Qian and Q. Chu, "A polarization-reconfigurable water-loaded microstrip antenna," *IEEE Antennas Wireless Propag. Lett.*, vol. 16, pp. 2179–2182, May 2017, doi: [10.1109/LAWP.2017.2703821](https://doi.org/10.1109/LAWP.2017.2703821).
- [24] A. H. Naqvi and S. Lim, "Microfluidically polarization-switchable metasurfaced antenna," *IEEE Antennas Wireless Propag. Lett.*, vol. 17, no. 12, pp. 2255–2259, Dec. 2018.
- [25] F. T. Ulaby and D. G. Long, *Microwave Radar and Radiometric Remote Sensing*. Ann Arbor, MI, USA: Univ. Michigan Press, 2014.
- [26] M. Haneishi and S. Yoshida, "A design method of circularly polarized rectangular microstrip antenna by one-point feed," *Electron. Commun. Japan I, Commun.*, vol. 64, no. 4, pp. 46–54, 1981.
- [27] R. Garg, *Microstrip Antenna Design Handbook*. Boston, MA, USA: Artech House, 2001.
- [28] J. R. James and P. S. Hall, *Handbook of Microstrip Antennas*, vol. 1. London, U.K.: IET, 1989.
- [29] H. Johnson, H. W. Johnson, and M. Graham, *High-Speed Signal Propagation: Advanced Black Magic*. Upper Saddle River, NJ, USA: Prentice Hall, 2003.
- [30] M. Biswas and M. Sen, "Fast and accurate model for a coax-fed rectangular patch antenna with varying aspect ratio, feed location and substrate electrical parameters," *J. Electromagn. Waves Appl.*, vol. 33, no. 4, pp. 428–453, 2019.
- [31] M. I. Pasha, C. Kumar, and D. Guha, "Application-friendly improved designs of single-fed circularly polarized microstrip antenna [antenna applications corner]," *IEEE Antennas Propag. Mag.*, vol. 61, no. 3, pp. 80–89, Jun. 2019.
- [32] M. Geissler, O. Litschke, D. Heberling, P. Waldow, and I. Wolff, "An improved method for measuring the radiation efficiency of mobile devices," in *IEEE Antennas Propagat. Soc. Int. Symp. Dig. Held Conjunction USNC/CNC/URSI North Amer. Radio Sci. Meeting*, vol. 4, 2003, pp. 743–746.
- [33] B. Y. Toh, R. Cahill, and V. F. Fusco, "Understanding and measuring circular polarization," *IEEE Trans. Edu.*, vol. 46, no. 3, pp. 313–318, Aug. 2003.
- [34] K.-L. Wong, C.-M. Chou, Y.-J. Yang, and K.-Y. Wang, "Multipolarized wideband circular patch antenna for fifth-generation multi-input-multi-output access-point application," *IEEE Antennas Wireless Propag. Lett.*, vol. 18, no. 10, pp. 2184–2188, Oct. 2019.
- [35] K. Saraswat and A. Harish, "A polarization reconfigurable cpw fed monopole antenna with l-shaped parasitic element," *Int. J. RF Microw. Comput.-Aided Eng.*, vol. 28, no. 6, 2018, Art. no. e21285.



**ADITYA SINGH** (Graduate Student Member, IEEE) received the Bachelor of Engineering (B.E.) degree in electronics and telecommunication engineering from Jabalpur Engineering College, Jabalpur, India, in 2012, and the Master of Technology (M.Tech.) degree in R.F. and microwave from the Indian Institute of Technology Kanpur, Kanpur, India, in 2014. He is currently pursuing the Ph.D. degree with the Department of Electrical and Computer Engineering, Queen's University, Kingston, ON, Canada. From 2014 to 2017, he was an Edison Engineer with General Electric, Bengaluru, India. His current research interests include antenna design for 5G systems, multiple-input-multiple-output antenna systems, and reconfigurable antenna design employing microfluidics. He was a recipient of the Ontario Trillium Scholarship from the Government of Ontario, Canada.



**CARLOS E. SAAVEDRA** received the B.Sc. degree in electrical engineering from the University of Virginia and the M.Sc. and Ph.D. degrees in electrical engineering from Cornell University, Ithaca, NY, USA.

He is a Professor and the Head of the Department of Electrical and Computer Engineering, Queen's University, Canada. During sabbatical leaves, he has held visiting appointments with the University of Navarra, Spain, the Universidade Federal de Rio Grande do Sul, Brazil, and the University of Twente, Holland. From 1998 to 2000, he was a Senior Engineer with Millitech Corporation, Northampton, MA, USA. He is Co-PI of the "Platform for Advanced Design Leading to Manufacturing in Micro-Nano Technologies," a multimillion dollar national infrastructure project funded by the Canada Foundation for Innovation and Provincial Governments.

Prof. Saavedra is a prior recipient of the Natural Sciences and Engineering Research Council of Canada (NSERC) Discovery Accelerator Award and is a three-time recipient of the ECE Undergraduate Teaching Award at Queen's University. He is a former Co-Chair of the NSERC Discovery Grant Evaluation Group for Electrical and Computer Engineering. He has served on grant review panels at the National Science Foundation, USA, and as an External Reviewer for the Netherlands Organization for Scientific Research. He is Guest Editor of the IEEE OPEN JOURNAL ON ANTENNAS AND PROPAGATION, and has previously served as an Associate Editor of the IEEE TRANSACTIONS ON MICROWAVE THEORY AND TECHNIQUES and as a Guest Editor of the *IEEE Microwave Magazine*. He is a licensed Professional Engineer (P.Eng.) in the Province of Ontario.